Noncircular tube spinning based on three-dimensional CAD model

Hirohiko Arai

National Institute of Advanced Industrial Science and Technology (AIST)

1-2-1 Namiki, Tsukuba, Ibaraki 305-8564 Japan

Email address: h.arai@aist.go.jp

Arai, Hirohiko. "Noncircular tube spinning based on three-dimensional CAD model." International Journal of Machine Tools and Manufacture 144 (2019): 103426.

https://doi.org/10.1016/j.ijmachtools.2019.103426

1. Introduction

In contrast to traditional metal spinning, which is used to form only circular products, the development of a spinning process for noncircular cross sections has been proceeding in recent years [1, 2]. For example, there is a strong need for the tube spinning of noncircular/non-axisymmetric shapes for the fabrication of automotive exhaust parts. Irie [3] developed a spinning machine with planetary rollers to manufacture eccentric/oblique exhaust tubes. The planetary rollers, whose radius of rotation changes to neck the tube end, are driven by a spindle around the workpiece while the workpiece is tilted and moved relative to the spindle axis to obtain the eccentric/oblique end. Xia et al. [4] conducted FEM simulations and experiments on this method. They reported a fracture caused by excessive radial feed and a crack caused by work hardening of the material in spinning experiments on eccentric shapes. These defects occurred on the inner side of the offset where the radial feed is maximum. Xia et al. [5] also investigated the effect of the forming parameters in this process.

However, this machine cannot form noncircular cross sections such as polygons or ellipses because the trajectory of the forming rollers is always circular even though it has offset or inclination. The review papers on spinning [1, 2] introduced various noncircular spinning methods that can

deal with such shapes. Therein, noncircular spinning was roughly categorized into two types: force-controlled spinning and synchronous spinning. Force-controlled spinning uses a noncircular mandrel and controls the pushing force of the roller. The roller follows the mandrel shape and the material is formed into the same shape as the mandrel. In synchronous spinning, the roller is numerically controlled to synchronize with the rotation angle of the spindle.

As synchronous spinning can form noncircular shapes without using a mandrel, it is suitable for tube spinning, and hence, in this study, we adopt synchronous spinning. Previous studies on synchronous spinning have resulted in the forming of various shapes. Shimizu [6] built a spinning machine for synchronous spinning using stepping motors and formed elliptic and square cones. In the study of Sekiguchi and Arai [7], the roller moved in the axial direction as well as the radial direction, synchronizing with the spindle rotation to form oblique and curved cones. Arai [8] applied synchronous spinning to tube necking and formed a square tube. Sugita and Arai [9] proposed synchronous multipass spinning, which gradually deforms a flat blank to a vertical wall over multiple passes to reduce thinning, and formed a square cup. Härtel and Laue [10] optimized the forming parameters to avoid wrinkling and thinning on the basis of FEM

simulations and formed a tripod shape. Russo and Loukaides [11] used internal rollers to support the workpiece instead of a mandrel. They analytically expressed the tool pass using several parameters and formed a square cup and a kidney-bean-shaped cup.

In the case of a dieless process in synchronous spinning, the product shape completely depends on the tool motion during forming. Transferring the part design into the motion program of the tool is an indispensable stage of the manufacturing process, although little attention has been paid to this stage so far in spite of the advances in the process of synchronous spinning. In particular, it is necessary to determine the position of the roller in contact with the target product to generate the NC command of the tool trajectory. The computation methods used in the previous works on synchronous spinning are revisited here from this viewpoint.

Shimizu [6] approximated the roller tool as an oblique planar circle and calculated the contact position with an elliptic cone. Arai [8] divided a target noncircular shape into layers of the planar cross-section shapes and geometrically calculated the contact position of the planar circular roller and a square with rounded corners. In these methods, a position error occurs owing to the thickness of the roller when the side wall of the target shape is not parallel to the roller axis. The cross sections are limited to specifically

defined shapes and cannot be generalized to arbitrary shapes. Sekiguchi and Arai [7] mathematically expressed oblique and curved cones and used a hemispherical tool bar as a roller to simplify the calculation of the contact position. Hence, this method is not suitable for the nonspherical rollers usually adopted in metal spinning. The compensation of the tool radius, which is generally used in a CAM system for incremental forming, cannot be applied for the same reason. Sugita and Arai [9] used force control to push the roller onto the mandrel and detected the contact position before the spinning process. This method requires a force control function and cannot be applied to dieless spinning without a mandrel, which is often used in tube necking. Russo and Loukaides [11] represented the shape of the product as a triangulated mesh and calculated the contact position of the roller in the plane containing the spindle axis by considering the shape of the intersection between the product and the plane. This method might involve a position error depending on the spindle rotation because the inclined noncircular surface does not always touch the roller on the plane including the spindle and roller axes. Thus, the interface between an arbitrary part design and the corresponding tool position is still an open problem in synchronous spinning.

In this paper, we propose a three-dimensional spinning method that uses

a 3D CAD model of the target product shape. The center position of the roller surface, which also has a point on the product surface, is geometrically calculated by considering the shape and dimensions of the roller. Then, the position where the roller is in contact with the target shape at a single point is searched for. Since the shape of the product can be expressed using a general-purpose CAD model, the tool trajectory can be calculated by a unified procedure from arbitrary design data even for a complex target shape. Not only the cross section perpendicular to the spindle axis but also the desired profile of the product in the axial direction can be obtained. In the experiments, eccentric, elliptic, oblique and square products are spun from aluminum tubes using this method, and the shape accuracy and thickness distribution obtained by this method are evaluated. In addition, it is demonstrated that the proposed method can form complex shapes by combining multiple elements with different shapes.

2. NC programming of 3D spinning

2.1 Calculation of roller contact position

Here, we explain the computation process used to geometrically calculate the contact position of the roller and the desired product shape for forming a noncircular shape by synchronous spinning. By considering the shape and dimensions of the roller tool, the roller position where the product and the

roller are in contact at a single point is obtained by a search algorithm.

The 3D model of the product surface is typically expressed by polygon data in, for example, the STL file format, which most current 3D CAD software can export. The polygon data can be easily converted into point cloud data consisting of numerous point coordinates on the surface. We assume that the rotation of the product is fixed and the axial position of the roller is constant. The roller moves only in the radial direction. When a point within the point cloud data is simultaneously located on the surface of the roller, the radial position of the roller can be geometrically calculated from the shape and dimensions of the roller. The radial position of the roller corresponding to each point cloud datum is calculated one after another. Among the calculated positions, the roller position that is most distant from the spindle axis is the position where the product and roller surfaces are in contact at only one point.

It is assumed that the spindle axis of the spinning lathe coincides with the z-axis of the absolute coordinate system. The roller moves parallel to the x-axis in the radial direction and parallel to the z-axis in the axial direction (Figure 1). The point P on the surface of the product shape is expressed as (x_s, y_s, z_s) in the coordinate system fixed to the product. P is given as an element of the point cloud data. Here, when the whole product

is rotated about the z-axis by an angle θ, P moves to P_θ $(x_\theta,\ y_\theta,\ z_\theta)$ in the absolute coordinate system, expressed as follows.

$$\begin{pmatrix} x_\theta \\ y_\theta \\ z_\theta \end{pmatrix} = \begin{pmatrix} \cos\theta & -\sin\theta & 0 \\ \sin\theta & \cos\theta & 0 \\ 0 & 0 & 1 \end{pmatrix} \begin{pmatrix} x_s \\ y_s \\ z_s \end{pmatrix} \qquad (1)$$

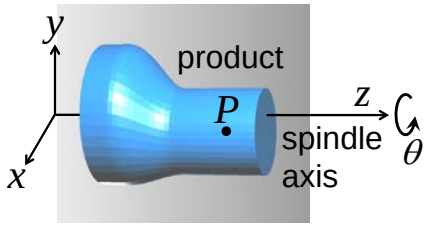

Figure 1 Product shape and absolute coordinate system

It is assumed that the roller is a wheel type and its shape is the outer circumference of a torus. The roller diameter is D and the radius of roundness is ρ. The radius of the center of roundness, R, is expressed as $R = \frac{D}{2} - \rho$ (Figure 2). The center of the roller moves on the xz plane and the roller axis is parallel to the z-axis. The coordinates of the roller center Q are $(x_R,\ 0,\ z_R)$. When the point P_θ $(x_\theta,\ y_\theta,\ z_\theta)$ on the product surface is in contact with the roller, the radius R_P of the roller surface at the contact point is

$$R_P = R + \sqrt{\rho^2 - (z_\theta - z_R)^2} \ . \qquad (2)$$

At this time, the x-coordinate x_R of the roller center Q is represented as

$$x_R = x_\theta + \sqrt{{R_P}^2 - {y_\theta}^2} \ . \qquad (3)$$

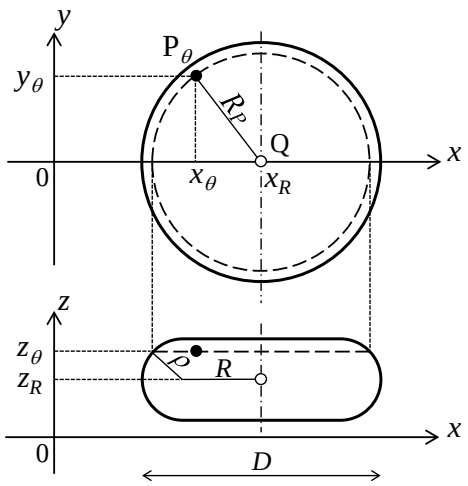

Figure 2 Relationship between point on product surface and roller

The position where the roller touches the product can be obtained by the following procedure. First, the rotation angle θ of the product shape and the axial position z_R of the roller are given. The point P_θ $(x_\theta,\ y_\theta,\ z_\theta)$ on the product surface rotated around the z-axis is calculated from Equation (1). Then, the radial position x_R of the roller is calculated from Equations (2) and (3). The contact point between the roller and the product can be in the range of $z_R - \rho \leq z_\theta \leq z_R + \rho$. x_R is calculated for all points belonging to the point cloud data within this range. The position where x_R is maximum is the single position where the roller touches the product.

The above search procedure is repeated while changing the rotation angle θ of the product and the axial position z_R of the roller, and the corresponding radial position $x_R(Z_R, \theta)$ of the roller is obtained over the

entire product surface (Figure 3).

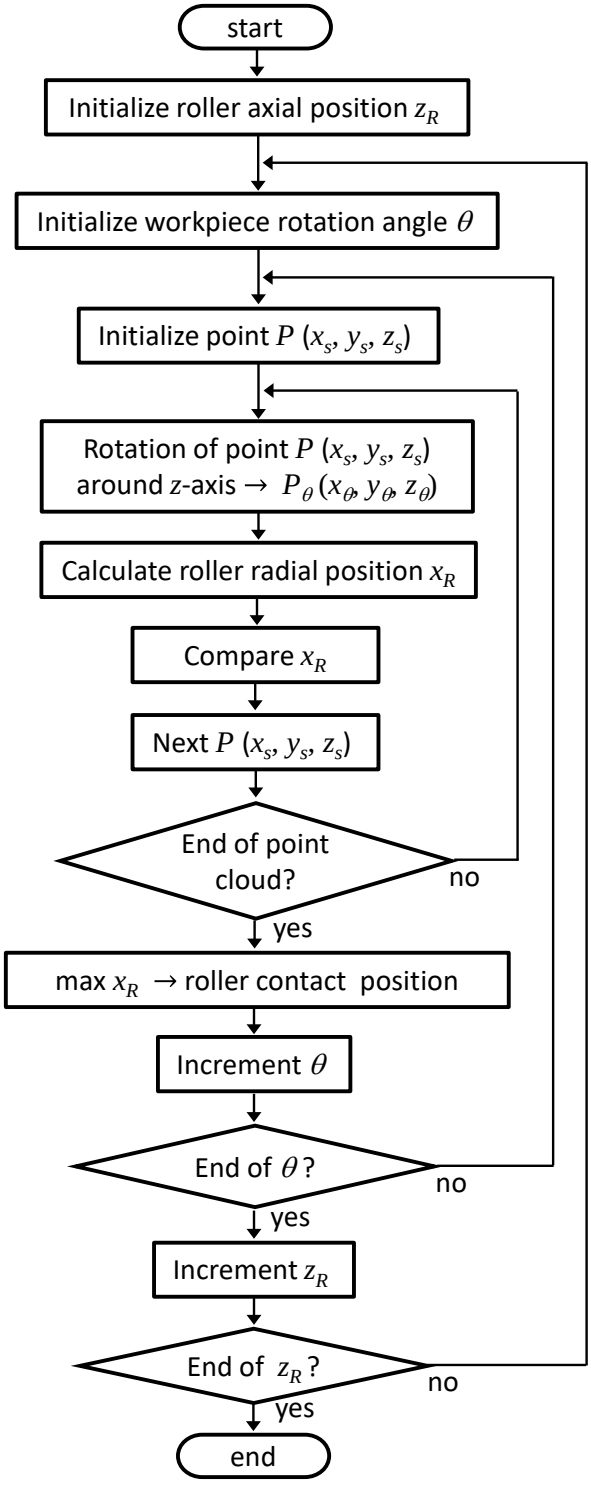

Figure 3 Computation algorithm of roller contact position

2.2 Evaluation of calculation accuracy

For the method in the previous subsection, the accuracy of the calculation result depends on the density of the point cloud data and the shape of the roller as the position of the roller is determined by a search algorithm. Here, it is verified that the obtained accuracy is suitable for the spinning process by calculating the roller position for a specific product shape using this method.

The shape used for the evaluation is an eccentric cylindrical shape with a diameter of 50 mm and a length of 50 mm, and the offset from the spindle axis is 10 mm. The density of the point cloud data is determined by the numbers of divisions in the circumferential and axial directions. Three classes of density, high density (120×120 divisions), medium density (60×60 divisions) and low density (40×40 divisions), are evaluated. Modela 3D Design (Roland DG Co.) 3D modeling software is used to create a 3D model and convert it to point cloud data.

The exact roller position for an eccentric cylindrical shape can be mathematically calculated as a reference value as follows:

$$x_{R\_ref} = l\cos\theta + \sqrt{(D/2 + d/2)^2 - (l\sin\theta)^2} \ , \qquad (4)$$

where l is the offset, D and d are the diameters of the roller and product, respectively, and θ is the rotation angle. The radial position x_R of the

roller is obtained by the proposed search method with an increment of 0.05 mm in the axial direction z_R of the roller and an increment of 1° in the rotation angle θ of the product shape. The deviation from the exact solution of Equation (4) is calculated for each position. The following three types of roller are used: large (diameter D= 200 mm, roundness radius ρ=10 mm), medium (D= 100 mm, ρ=5 mm) and small (D= 50 mm, ρ=2.5 mm). The maximum error $\left|x_R - x_{R\_ref}\right|_{MAX}$ is plotted in Figure 4.

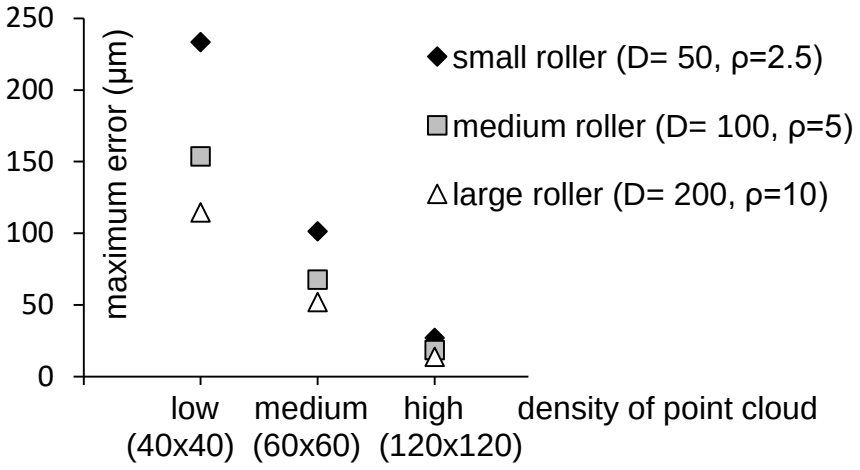

Figure 4 Maximum error of roller radial position

As the size of the roller and the density of the point cloud data increase, the position error of the roller tends to decrease. The distance of the roller from the spindle axis is always smaller than the exact solution. This is

because the point cloud is discrete, whereas the product surface is actually continuous. There exists a contact point on the product surface outside the point cloud that gives a larger radial position x_R than the maximum x_R given by the contact point within the point cloud. The roller position error with respect to the point cloud data of high density (120×120 divisions) is less than 30 μm for all rollers. Considering the forming precision of the spinning process in general, sufficient accuracy of the roller position is obtained by the proposed method.

2.3 Tool position in synchronous multipass spinning

Usually, tube necking by spinning is performed with multiple passes to prevent failures such as excessive thinning, wrinkling and fracture. The roller should move reciprocally between the tip end and the base end in the axial direction while approaching the target shape in the radial direction. Sugita and Arai [9] proposed synchronous multipass spinning to form a square cup from a sheet blank. It combined synchronous spinning with multipass spinning to gradually change the workpiece shape from a flat blank to the noncircular target shape. Arai [8] also applied synchronous multipass spinning to tube necking. Here, the computation method used to calculate the NC command from the positions where the roller is in contact with the product and with the blank tube is reviewed briefly.

The axial and radial components of the position where the roller is in contact with the product, obtained by the method in subsection 2.1, are denoted as z_k and $x_{p\_k}(\theta)$ $(k = 1, \cdots, n)$, respectively, where θ is the rotation angle of the spindle and n is the number of axial positions. z_1 is the axial position of the tip end of the product and z_n is that of the base end. The radial position for the blank tube at z_k is also defined as $x_{b\_k}(\theta)$ $(k = 1, \cdots, n)$. When the blank is a cylindrical tube, $x_{b\_k}(\theta)$ is constant.

Next, multiple tool paths are defined on a virtual two-dimensional plane (Figure 5). The virtual plane is normalized from 0 to 1 in the axial direction s_z and radial direction s_x of the workpiece. $s_z = 0$ represents the tip end of the product and $s_z = 1$ represents the base end. When $s_x = 1$, the roller moves along the surface of the blank tube, and when $s_x = 0$, it moves along the product surface. The normalized path is composed of curved and straight path elements. The curved path is a part of a sine curve scaled in the s_x and s_z directions to fit the start and end points.

Finally, the actual tool position (x_t, z_t) corresponding to a point (s_x, s_z) on the normalized tool path is calculated by linear interpolation. The tool position z_t in the axial direction is obtained from s_z as

$$z_t = z_1 + (z_n - z_1)s_z \ . \qquad (5)$$

The radial position $x_p(s_z, \theta)$ of contact with the product corresponding to the

axial displacement s_z on the normalized path is calculated by the linear interpolation of $x_{p\_k}(\theta)$ $(k = 1, \cdots, n)$ using s_z as an interpolation coefficient. The radial position $x_b(s_z, \theta)$ of contact with the blank is also calculated in the same manner.

Then, the radial positions of the contacts, $x_p(s_z, \theta)$ and $x_b(s_z, \theta)$, are interpolated using s_x as an interpolation coefficient to obtain the intermediate radial position x_t as follows

$$x_t = s_x x_b(s_z, \theta) + (1 - s_x) x_p(s_z, \theta) \ . \qquad (6)$$

This calculation procedure for the tool position (x_t, z_t) is sequentially performed along the normalized paths to generate the entire trajectory. The series of roller positions and spindle angles (x_t, z_t, θ) thus obtained are connected by NC commands of linear interpolation motion, for example, "G01" in G code.

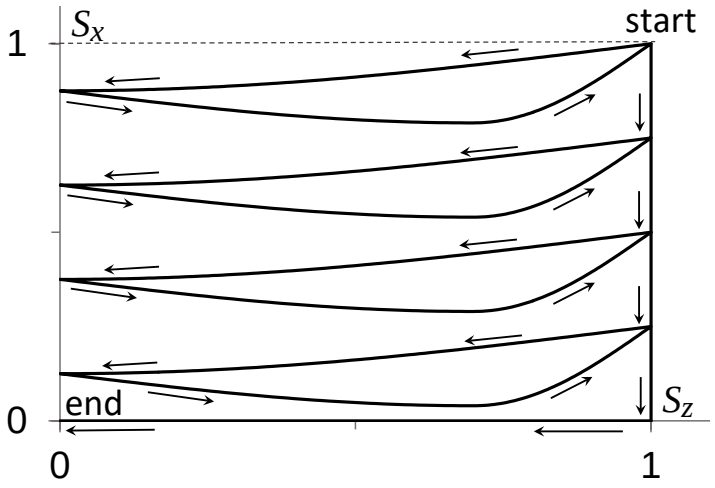

Figure 5 Example of normalized tool path

3. Experimental conditions

The element shapes that compose the 3D model of the target product are generated using 123D Design (Autodesk, Inc.) and Modela 3D Design (Roland DG Co.) 3D modeling software. A 3D model of the product shape is edited by 3D Editor (Roland DG Co.) to adjust the positional relationship between the elements to export polygon data in STL format. The STL data are converted into point cloud data with sufficient density, and the contact position of the roller is searched for by considering the geometry of the roller. The proposed algorithm is programmed in C language and implemented on a Windows personal computer.

A five-axis CNC spinning machine with two rollers is used in our spinning experiments. The roller tool has a diameter of 88 mm and a roundness radius of 4 mm. The blank is a pure aluminum tube (A 1050 TD - H) with a diameter of 50 mm, a thickness of 1.55 mm and a length of 100 mm. Compressor oil (ISO VG 68) is used for lubrication between the roller and the workpiece.

Four noncircular shapes, namely, eccentric, elliptic, oblique and square, are formed. The tip portion of the workpiece is necked from a circular tube to the desired shape in every case. For the eccentric shape, the necked cross section has a diameter of 30 mm and an offset of 2, 4, 6 or 8 mm. The

elliptic shape has a minor axis of 30 mm length and a major axis of 34, 38, 42 or 46 mm length. The necked portion of the oblique shape has a diameter of 30 mm and the oblique angle is 10, 15, 20, 25 or 30°. The square shape has a square cross section with a side of 35 mm length and the roundness of the corners is 2, 3, 4, 6 or 10 mm. For the eccentric, elliptic and oblique shapes, the contact position of the roller is calculated at 60 points per rotation, i.e., for every 6° rotation of the workpiece. For the square tube, the calculation is performed at 120 points per rotation, i.e., for every 3°. The number of roller passes is 7 roundtrips, i.e. 14 passes. The axial roller feed is 2 mm/rev except for the final pass, which has a 1 mm/rev roller feed. The spindle speed is 60 rpm for the eccentric, elliptic and oblique shapes and 30 rpm for the square shape. The shape of each product is measured using a laser rangefinder of 0.5 μm resolution. The wall thickness is measured using a micrometer.

4. Evaluation of forming results

4.1 Eccentric shape

The products with the eccentric shape are shown in Figure 6, and the offset of the product axis is compared with the target value in Figure 7. The axes of the products have offsets nearly equal to the target value, and the

offsets tend to be slightly smaller than the target value. The larger the offset becomes, the larger the error becomes. The maximum error is 0.14 mm when the offset is 8 mm. The average diameter of the necked part is 29.95 mm and the out-of-roundness is 0.16 mm when the offset is 8 mm.

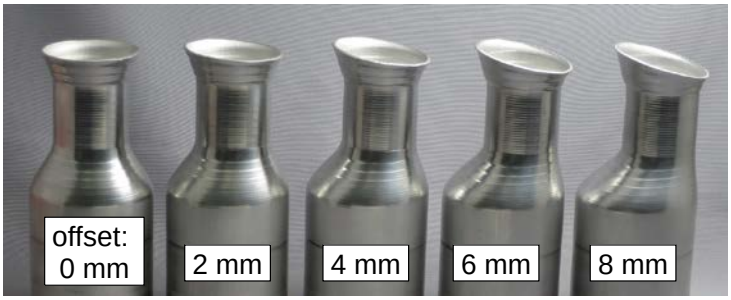

Figure 6 Products with eccentric shape

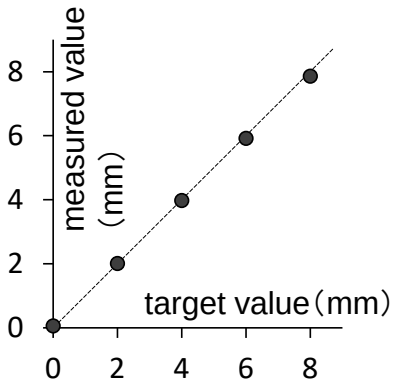

Figure 7 Offset of target and product shapes

Figure 8 shows the circumferential distribution of the wall thickness when the offset is 8 mm. On the inner side in the eccentric direction (180°),

where the deformation is maximal, the thickness is significantly greater than that on the outer side (0°). The thickness distribution in the axial direction for 8 mm offset is shown in Figure 9. The horizontal axis is the distance from the base end of the necked portion. The wall thicknesses on the inner and outer sides markedly differ near the base end. The difference becomes smaller as the axial position approaches the tip. Figure 10 shows the change in wall thickness versus the offset at the same axial position. In the case of the circular shape, i.e., the offset is zero, the wall thickness uniformly increases. As the offset increases, the wall thickness on the inner side (180°) increases, while that on the outer side (0°) approaches the blank thickness.

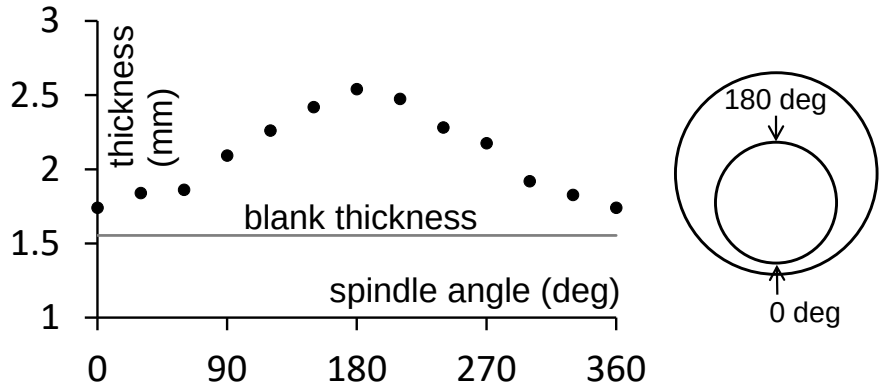

Figure 8 Circumferential thickness distribution of eccentric shape

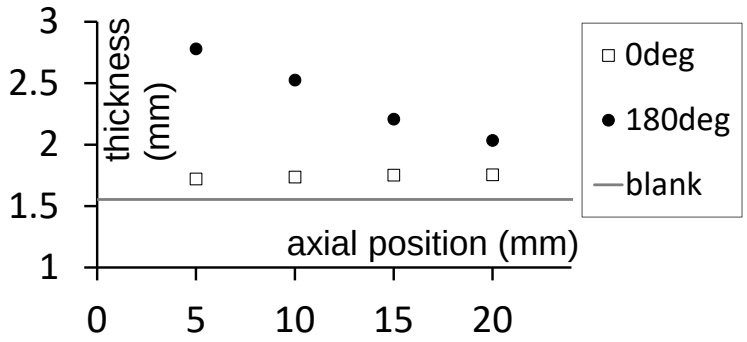

Figure 9 Axial thickness distribution of eccentric shape

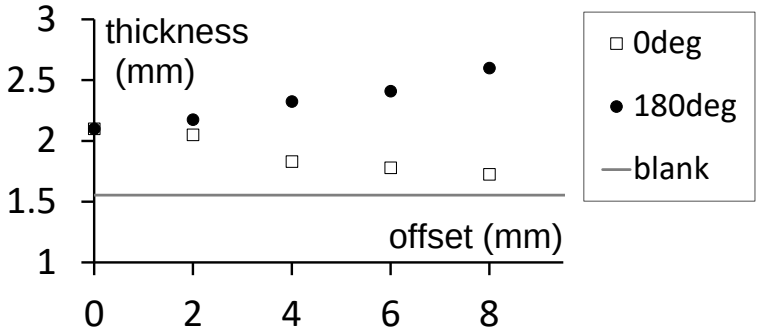

Figure 10 Relationship between offset and thickness distribution

4.2 Elliptic shape

The products with the elliptic shape are shown in Figure 11. Figure 12 shows the cross section of the product when the major diameter is 46 mm. Although there is some deviation from the target shape (thin solid line) near both ends of the major axis, the product is formed roughly in accordance with the target shape. The major diameter of the product is compared with the target diameter in Figure 13. The major diameter is slightly smaller than the target value, and the longer the diameter, the larger the error. The

maximum error is 0.48 mm when the major diameter is 46 mm.

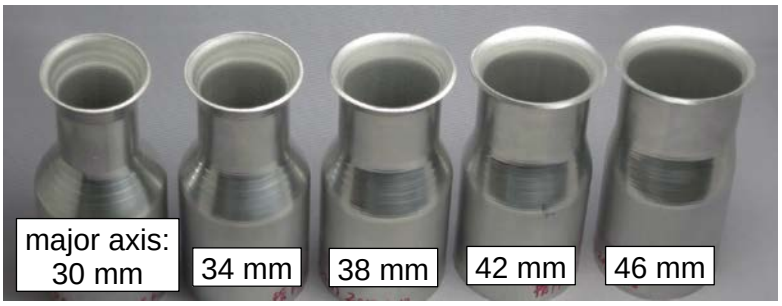

Figure 11 Products with elliptic shape

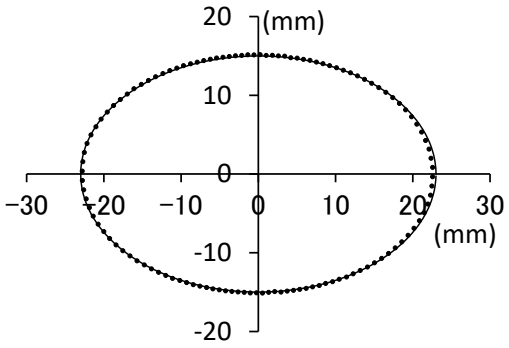

Figure 12 Cross section of elliptic shape

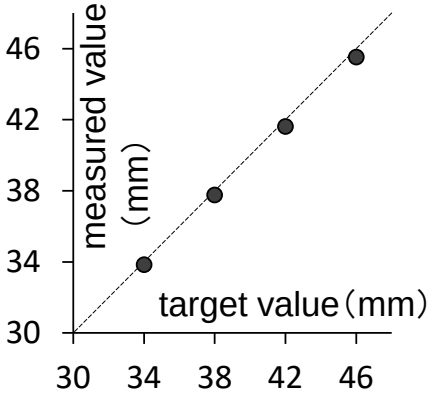

Figure 13 Major diameter of target shape and products

Figure 14 shows the wall thicknesses at the ends of major and minor axes versus the major diameter. Although the wall thickness tends to be larger at the end of the major axis than at the end of the minor axis, notable difference in wall thickness is not observed, as in the case of the eccentric shape.

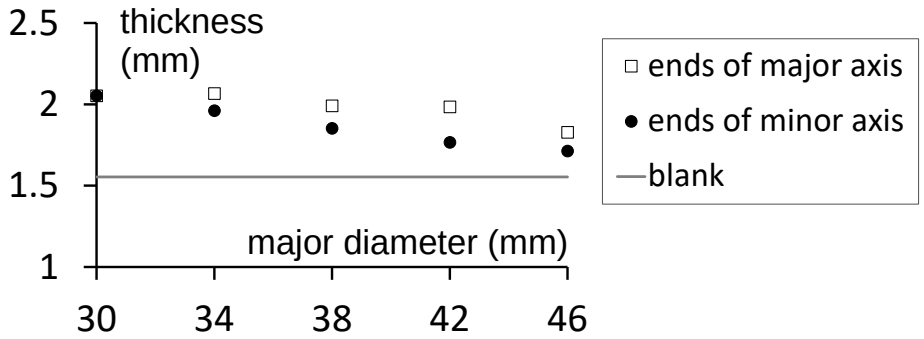

Figure 14 Major diameter and wall thickness of elliptic shape

4.3 Oblique shape

Figure 15 shows the products with the oblique shape. When the oblique angle is 30°, the tip end of the target shape lies outside the periphery of the blank tube. However, the tip end of the product does not lie outside the periphery and the original surface of the blank remains unformed (Figure 16). This means that the formability of a noncircular shape by tube necking is limited to the inside of the blank tube. The oblique angles of the product axis and target shape are compared in Figure 17. The oblique angle of the

product that is almost equal to the target value is achieved. The maximum error of the oblique angle is 0.93° when the target value is 30°.

Figure 15 Products with oblique shape

Figure 16 Tip end of 30° oblique shape

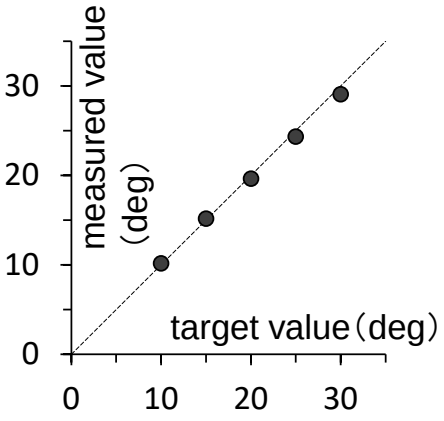

Figure 17 Oblique angles of target shape and product

The thickness distribution in the axial direction when the oblique angle is 25° is shown in Figure 18. The horizontal axis is the distance from the base end of the necked portion. The thickness on the inner side (180°) becomes progressively thinner than the blank thickness as the axial position approaches the base, in contrast to the thickening observed for the eccentric shape in Figure 10.

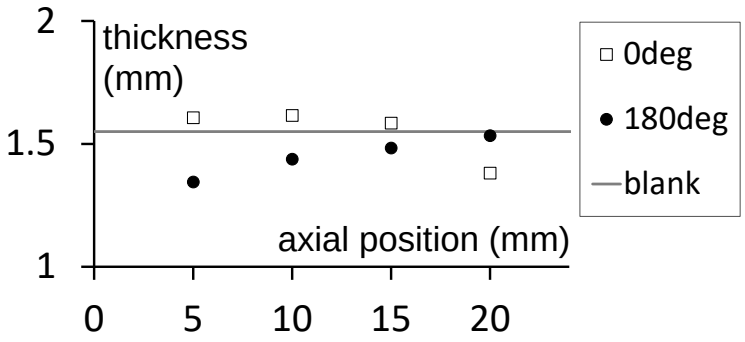

Figure 18 Axial thickness distribution of oblique shape

4.4 Square shape

Figure 19 shows the square tube products, and Figure 20 shows the measurement result of the cross section when the roundness of the corners is 4 mm. The product is formed in accordance with the target square shape (thin solid line). The distance between the opposite sides of the square tends to be larger than the desired value of 35 mm by 0.33 to 0.43 mm. The roundness of the corners is visually verified using radius gauges, and the

radius error is less than the increment of the gauges, 0.5 mm, in all cases. At roundnesses of 2 and 3 mm, peeling of the surface material is observed in the vicinity of the corner (Figure 21). Peeling takes place only on one side of the corner, which corresponds to the area where the roller moves towards the workpiece; thus it is considered that the contact force becomes excessive there.

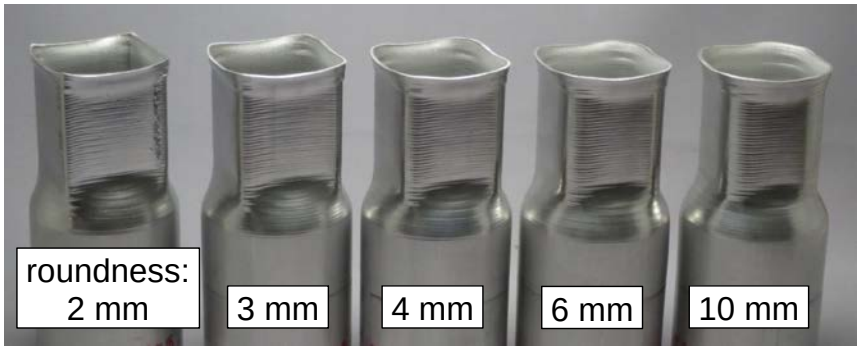

Figure 19 Products with square shape

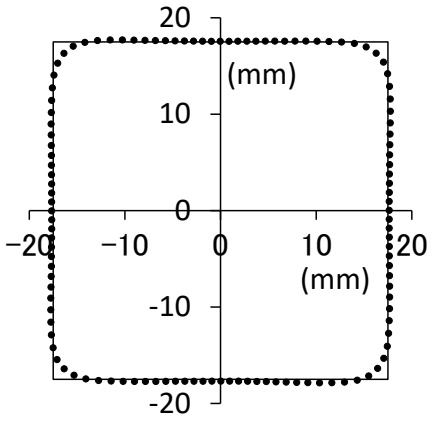

Figure 20 Cross section of square shape

Figure 21 Peeling of surface material

Figure 22 shows the circumferential thickness distributions for corner roundnesses of 2, 6 and 10 mm. The horizontal axis is the distance from the midpoint of the side. The values at both ends represent the wall thickness at the corners. The corner has a larger thickness, and the thickness at the midpoint is slightly smaller than that of the blank tube. Regardless of the size of the roundness, the thickness of the corner is nearly the same. When the roundness is small, the thickness of the side is almost constant, but when the roundness increases, the thickness of the side also continuously changes.

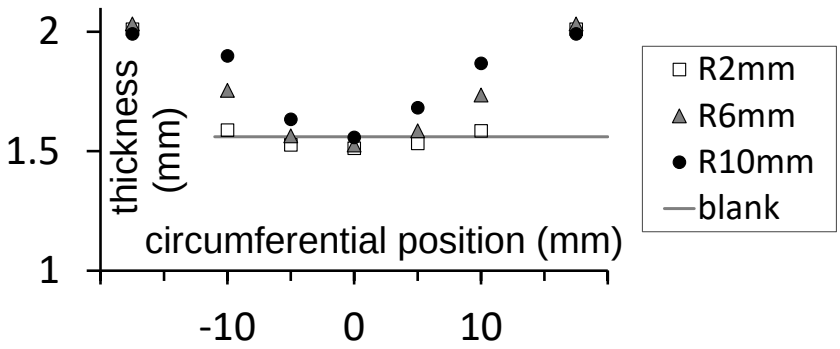

Figure 22 Circumferential thickness distributions of square shape

4.5 Effect of forming parameters

The effect of the forming parameters on the dimensional accuracy of the product is investigated for an eccentric shape. The out-of-roundness of the necked portion is measured for different parameters when the necked diameter is 30 mm and the offset is 8 mm. The changed parameters are 1) the axial roller feed per rotation, 2) the number of passes and 3) the rotation speed of the spindle. Figures 23, 24 and 25 show the plots of the out-of-roundness versus these forming parameters. While the axial roller feed and spindle speed do not clearly affect the out-of-roundness, the roundness markedly deteriorates as the number of passes decreases.

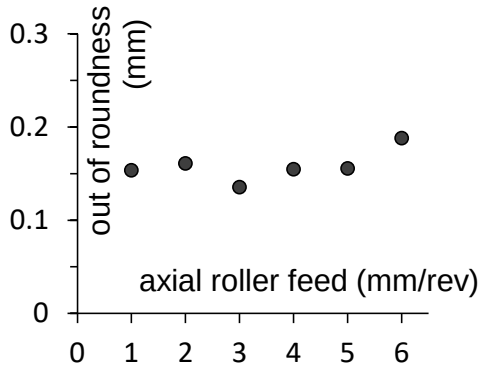

Figure 23 Relationship between axial roller feed and roundness

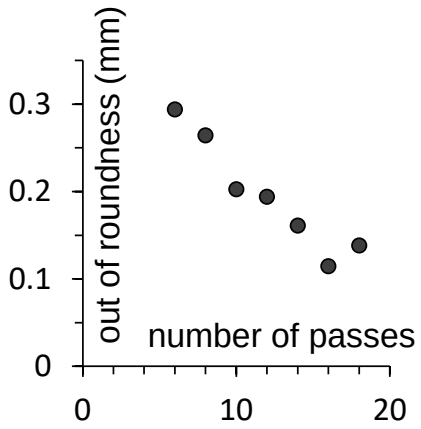

Figure 24 Relationship between number of passes and roundness

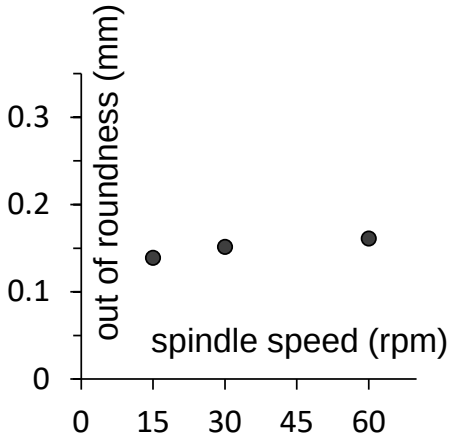

Figure 25 Relationship between spindle speed and roundness

When the eccentric shape is spun with a small number of passes, the diameter through the inner side (180°) and the outer side (0°) becomes smaller than the target diameter whereas the diameter perpendicular to it is nearly equal to the target value. During the spinning process, it is observed

that the roller leaves the surface of the inner side when the workpiece is spun with the final pass. As the roller does not touch the workpiece, the product cannot be formed into the target shape at that portion even if the roller follows the contact position with the target shape.

To investigate the reason for this defect, the change in the axial profile of the inner side (180°) is measured at the final stage of forming. The number of passes is three roundtrips, i.e., six passes. The axial roller feed is 2 mm/rev for the first to fifth passes and 1 mm/rev for the sixth pass. Three samples are measured: the workpiece after the fifth pass, the workpiece when forming is interrupted in the middle of the sixth pass, and the workpiece after the sixth pass.

Figure 26 shows a plot of the measured profile of each sample. The surface of the workpiece after the fifth pass (blue dots) has some margin to the target shape of the 3D model (gray line). When the roller proceeds from the base up to the red triangle along the sixth pass, the profile of the tip side falls below the target profile even though the roller has not yet pushed that portion (red dots). This means that the workpiece is bent downward near the red triangle. When the sixth pass is completed (green dots), the roller and workpiece have a gap between them and the product shape has a dimensional error relative to the target shape.

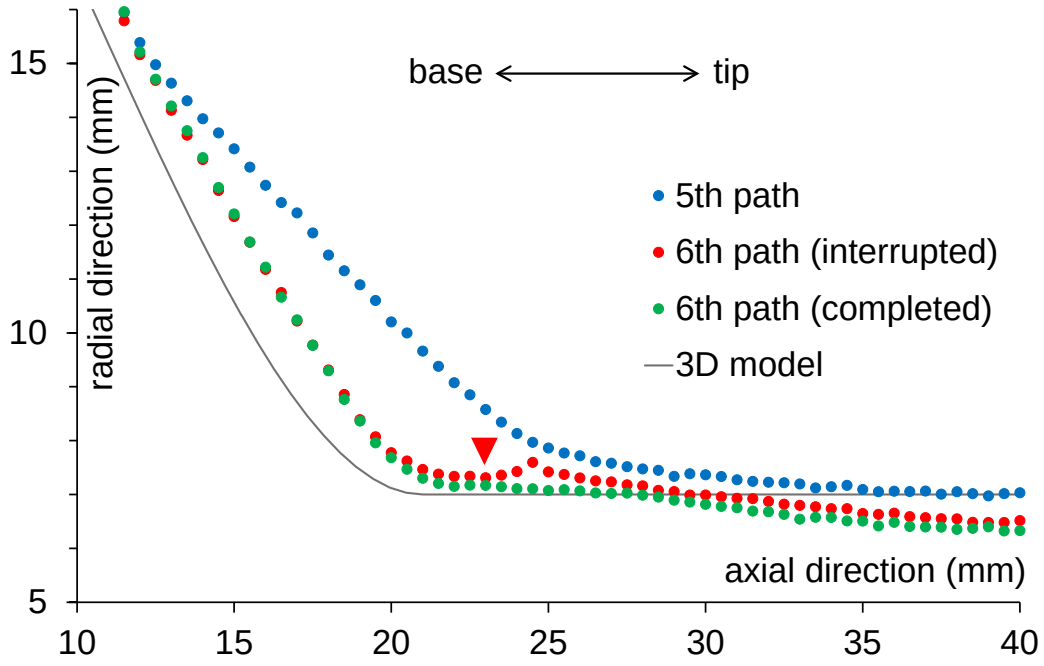

Figure 26 Change of axial profile in forming eccentric shape with small number of passes

Such bending behavior is considered to be caused by the unbalanced axial elongation. As can be seen from Figure 6, the tip of the eccentric shape is inclined because the elongation of the necked portion is not uniform. The inner side stretches more than the outer side because the radial feed of the inner side in each pass is larger than that of the outer side. Such an asymmetrical elongation of an eccentric shape was also reported in Ref. [4]. When the radial feed of the inner side is excessively larger than that of the outer side, the difference in elongation seems to generate a moment that bends the workpiece beyond the target shape.

Figure 9 shows that the wall of the inner side of the eccentric shape is thicker than the outer side, but the difference becomes smaller as the axial position approaches the tip. This can also be interpreted by the bending of the workpiece. In the case of Figure 9, the number of passes is 14 and the bending is not sufficiently large to result in a dimensional error. However, the slight inclination towards the outer side makes the radial deformation of the outer side larger and that of the inner side smaller in each pass. Therefore, the wall thickness of the tip becomes more uniform than the base.

Similar bending behavior can also be observed in the forming of an oblique shape. An oblique shape with an oblique angle of 20° is spun with six passes to a diameter of 30 mm. The axial profiles after the fifth pass (blue dots), interrupted in the middle of the sixth pass (red dots) and after the sixth pass (green dots) are measured (Figure 27). Similarly to the eccentric shape, when the roller proceeds from the base to the red triangle in the sixth pass, the tip of the workpiece inclines towards the outer side beyond the target profile. Consequently, the final profile after the sixth pass deviates from the target profile.

In summary, the asymmetry of the radial feed in noncircular spinning leads to uneven axial elongation, depending on the circumferential location. The bias of the axial elongation can bend the workpiece during the spinning

process and it may affect the dimensional accuracy and thickness distribution. The forming parameters including the number of passes should be chosen so that such an adverse effect on the forming quality can be avoided.

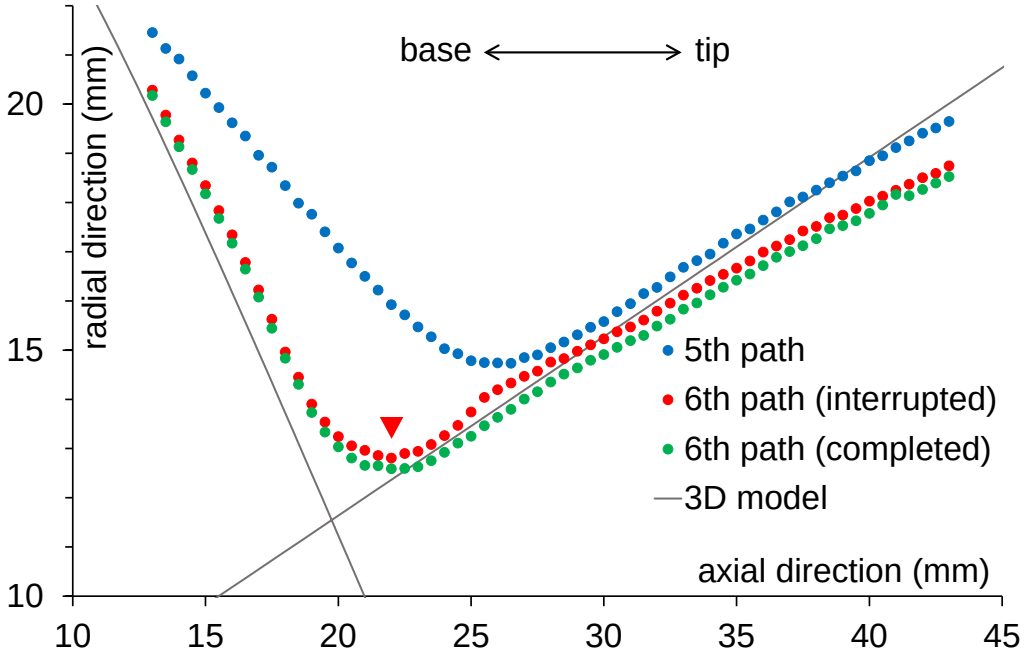

Figure 27 Change of axial profile in forming oblique shape with small number of passes

5. Complex shapes

Finally, two sample products with complex shapes consisting of several elements with different shapes are formed to demonstrate the flexibility of the proposed method. Sample A is composed of two spheres of 35 mm diameter, a sphere of 50 mm diameter and a cylinder of 25 mm diameter. The two 35 mm spheres are arranged asymmetrically. Sample B is composed of a cube of 35 mm sides with fillets of 8 mm radius and a triangular prism of 38 mm sides with fillets of 7 mm radius. The cube is inclined so that one of the internal diagonals overlaps with the z-axis. The 3D model of Sample A consists of 35,878 triangular polygons and that of Sample B consists of 17,056 polygons. These polygon models are converted into point cloud data of 83,477 points and 57,416 points, respectively. The contact position of the roller is calculated at 60 points per rotation and at 60 layers in the axial direction by the proposed method. The computation takes 9 s for Sample A and 7 s for sample B using a Windows personal computer (Intel Core i7 CPU, 3.6 GHz). The processing time is sufficiently short for practical use.

The number of roller passes is 15 roundtrips. Figure 28 shows the normalized paths and the actual roller paths at 0 and 180° for Sample A. The axial roller feed is 2 mm/rev except in the final pass, where it is 1

mm/rev feed. The forming process takes 16 min for sample A and 26 min for Sample B. Figure 29 shows the formed products (right) and solid images of the 3D models (left). Both samples are formed into the same shape as the corresponding 3D model. Figure 30 shows the axial profiles of the products (black dots) and 3D models (gray thin lines) at 0 and 180°. The desired profile is mostly achieved in both samples.

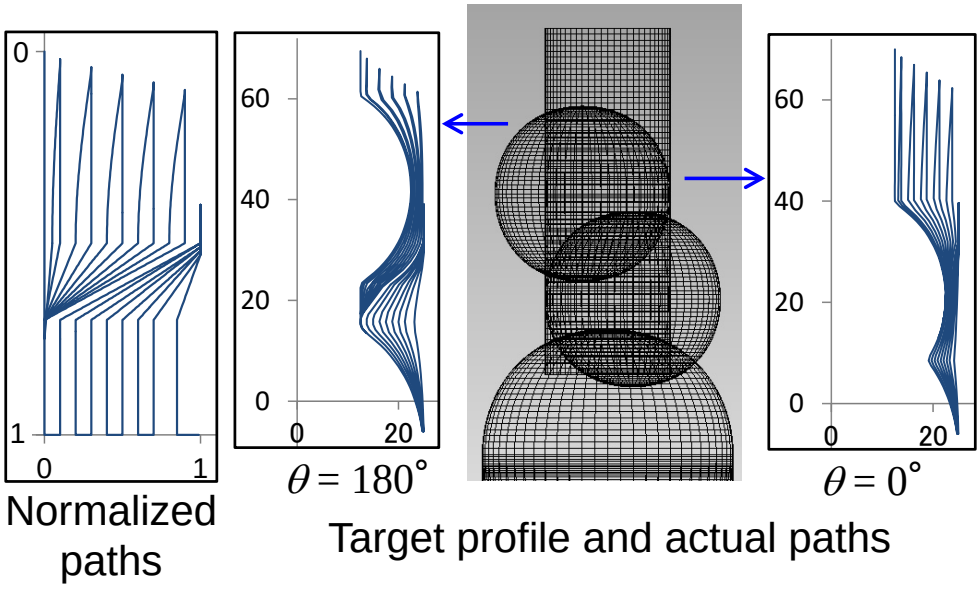

Figure 28 Normalized paths and actual roller paths of Sample A

(a) Sample A

(b) Sample B

Figure 29 3D models and products with complex shapes

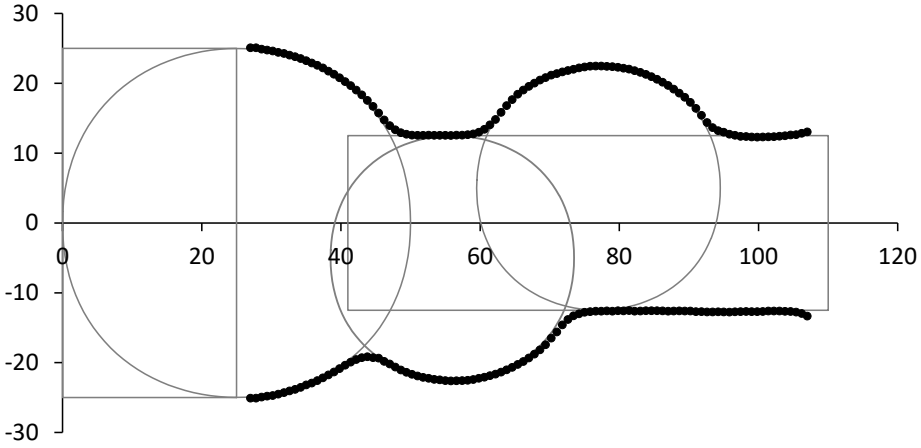

(b) Sample A

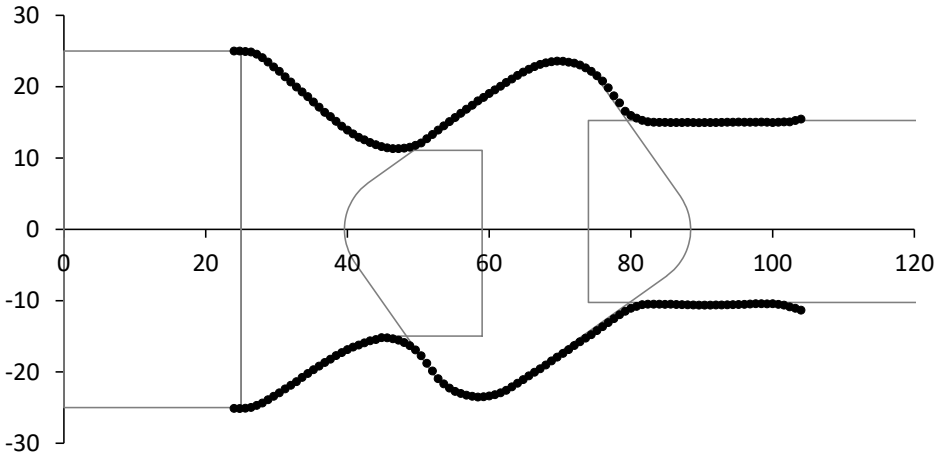

(b) Sample B

Figure 30 Axial profiles of complex-shaped products

6. Conclusions

A noncircular tube necking method is proposed, in which the position where the roller touches the target product shape is calculated using a 3D CAD model. The product shape is represented as a point cloud exported

from the 3D CAD software. Considering the geometry of the roller, the position of the roller in contact with each point cloud datum is calculated. The position of the single point where the roller and product surface meet is determined by a search algorithm. The experimental results for eccentric, elliptic, oblique and square shapes spun from aluminum tubes show that the product shapes are formed into almost the same shape as the corresponding 3D model. Two complex shapes combining several elements with different shapes are successfully formed by this method. This method can deal with any target shape freely, provided that it is formable by spinning. The human workload of NC programming for noncircular spinning is greatly reduced through the use of the proposed method. The desired axial profile as well as the cross section perpendicular to the spindle axis can be achieved.

However, the asymmetry of the radial feed in noncircular spinning may cause uneven axial elongation, and it can bend the workpiece and affect the dimensional accuracy. The forming parameters should be selected to prevent such an undesirable effect.

References

[1] Music, O., Allwood, K., J., and Kawai, K., 2010. A review of the mechanics of metal spinning. Journal of Materials Processing Technology 219, 3-23 https://doi.org/10.1016/j.jmatprotec.2009.08.021

[2] Xia, Q., Xiao, G., Long, H., Cheng, X., Sheng, X., 2014. A review of process advancement of novel metal spinning, Int. J. Machine Tools and Manufacture, 85, pp. 100-121. https://doi.org/10.1016/j.ijmachtools.2014.05.005

[3] Irie,T., 2001. Method and apparatus for forming a processed portion of a workpiece. United States Patent, US6223993B1, May 22, 2001.

[4] Xia, Q., Xie, S., Huo, Y., Ruan, F., 2008. Numerical simulation and experimental research on the multi-pass neck-spinning of non-axisymmetric offset tube, J. Mater. Process. Technol. 206 (1–3), pp. 500-508. https://doi.org/10.1016/j.jmatprotec.2007.12.066

[5] Xia, Q., Cheng, X., Long, H., Ruan, F., 2012. Finite element analysis and experimental investigation on deformation mechanism of non-axisymmetric tube spinning, Int. J. Adv. Manuf. Technol., 59 (1–4), pp. 263–272. https://doi.org/10.1007/s00170-011-3494-0

[6] Shimizu, I., 2010. Asymmetric forming of aluminum sheets by synchronous spinning. J. Mater. Process. Technol. 210, pp. 585–592.

https://doi.org/10.1016/j.jmatprotec.2009.11.002

[7] Sekiguchi, A., Arai, H., 2010. Synchronous die-less spinning of curved products. Steel Research International, 81 (9), pp. 1010–1013. https://doi.org/10.1002/srin.201190002

[8] Arai, H., 2014. NC programming for noncircular tube necking using synchronous multipass spinning. In: Proceedings of 2014 Japanese Spring Conference for the Technology of Plasticity, Tsukuba, Japan, pp. 199–200. (in Japanese)

[9] Sugita, Y., Arai, H., 2015. Formability in synchronous multipass spinning using simple pass set, J. Mater. Process. Technol. 217, pp. 336–344. https://doi.org/10.1016/j.jmatprotec.2014.11.017

[10] Härtel, S., Laue, R., 2016. An optimization approach in non-circular spinning, J. Mater. Process. Technol. 229, pp. 417–430. https://doi.org/10.1016/j.jmatprotec.2015.09.003

[11] Russo, I., Loukaides, E., 2017. Toolpath generation for asymmetric mandrel-free spinning. Procedia Engineering. 207, pp. 1707–1712. https://doi.org/10.1016/j.proeng.2017.10.926

Acknowledgement

This work was partially supported by Daito Spinning Co., Ltd.